# AXIAL RF ELECTRIC FIELD INTENSITY AND ION DENSITY DURING LOW TO HIGH MODE TRANSITION IN ARGON ELECTRON CYCLOTRON RESONANCE DISCHARGES

by

D. A. Carl, M. C. Williamson, M. A. Lieberman,
and A. J. Lichtenberg

Memorandum No. UCB/ERL M90/81

12 September 1990

COVER PAGE

# AXIAL RF ELECTRIC FIELD INTENSITY AND ION DENSITY DURING LOW TO HIGH MODE TRANSITION IN ARGON ELECTRON CYCLOTRON RESONANCE DISCHARGES

by

D. A. Carl, M. C. Williamson, M. A. Lieberman,
and A. J. Lichtenberg

Memorandum No. UCB/ERL M90/81

12 September 1990

**ELECTRONICS RESEARCH LABORATORY**

College of Engineering
University of California, Berkeley
94720

# AXIAL RF ELECTRIC FIELD INTENSITY AND ION DENSITY DURING LOW TO HIGH MODE TRANSITION IN ARGON ELECTRON CYCLOTRON RESONANCE DISCHARGES

by

D. A. Carl, M. C. Williamson, M. A. Lieberman,
and A. J. Lichtenberg

Memorandum No. UCB/ERL M90/81

12 September 1990

**ELECTRONICS RESEARCH LABORATORY**

College of Engineering
University of California, Berkeley
94720

**Axial rf electric field intensity and ion density during low to high mode transition in argon electron cyclotron resonance discharges**

D. A. Carl (Dept. of Chemical Engineering)

M. C. Williamson, M. A. Lieberman, and A. J. Lichtenberg
(Dept. of Electrical Engineering and Computer Sciences)

Plasma Assisted Materials Processing Laboratory
University of California
Berkeley, CA 94720

## ABSTRACT

To investigate the transition from the low density mode to the high density mode in an electron cyclotron resonance (ECR) discharge, a Langmuir probe and an E field probe were used to measure ion density and E field intensity as functions of axial position and power. The experiments were performed in argon at 0.13 Pa in a 7.9 cm D cylindrical source chamber propagating $TE_{11}$ mode 2.45 GHz microwave power. Low mode was characterized by a standing wave throughout the plasma chamber and minimal power absorption. High mode exhibited nearly complete power absorption and no standing wave past the ECR zone. A sliding short (ss) was used to determine if the position of an E field null in the source chamber affected the transition between these two modes for various magnetic field configurations. The ss position had little effect on mode transition, relative power absorption or ion density when positioned downstream from a broad, large volume resonance zone (resonance near the mirror midplane). However, the plasma could not be ignited if the short was placed at or upstream from the large volume resonance zone. If the magnetic field was adjusted to yield a sharp, small volume resonance zone (resonance midway between the midplane and the throat), then positioning the ss to force an E field null at the resonance zone would prevent plasma ignition, even at 800 W forward power. The ion density exhibited a hysteresis (i.e. a direct jump from no plasma to a plasma density observed at other sliding short positions for that same forward power, thereafter following the ion density vs. forward power dependence observed at nearby ss positions) on power cycling when the sliding short

was within approximately 1 cm of the broad resonance zone or within approximately 1 cm of forcing a null in the sharp resonance zone cases. The ion density vs. power curve for the broad volume case exhibited a change in slope over the transition region ($P_{forward} \approx 40$ W) when the ion density at the resonance zone was $\approx 1 \times 10^{11}$ $cm^{-3}$. For the narrow zone cases, a region of bi-stability (i.e. rapid plasma density fluctuations between low and high mode with little or no change in external input power) was observed for which the ion density fluctuated between a value near $5 \times 10^{10}$ $cm^{-3}$ in low mode and $5 \times 10^{11}$ $cm^{-3}$ in high mode. Similar transitions were observed in a 14.6 cm D ECR source with a $TM_{01}$ mode, indicating that the effect is not solely dependent on the microwave field structure in the ECR chamber.

## I. INTRODUCTION

ECR plasma processing of materials has been an area of recent intense research efforts. One interesting aspect of these plasmas is that they can be operated stably in several equilibrium plasma modes.[1-7]. There appear to be two primary modes of operation in such systems, hereafter referred to as low and high. Low mode is characterized by low fractional power absorption by the plasma and consequently low ion density in the resonance zone ( $< 10^{11}$ $cm^{-3}$), a standing wave in the chamber past the ECR resonance zone, and low photoemission intensity. High mode is characterized by nearly complete power absorption at the resonance zone, no standing wave pattern past the resonance zone, high resonance zone ion density ($>10^{11}$ $cm^{-3}$) that is a linear function of input power, and high photoemission intensity (10 to 30 times greater than low mode intensities for a given emission line as a consequence of the higher electron density). The transition from low to high mode or from high to low mode can be effected by small changes in input power (at low powers) or by changing the matching network tuning stub position.

Understanding this mode transition is critical to ensure proper reactor design and subsequent process control of materials modification. To improve our understanding of this phenomena, we constructed a sliding short (ss) in the ECR chamber to control the phase of electromagnetic reflections and therefore the position of field nulls in the chamber. The field pattern was measured and correlated with changes in the electron density vs. power characteristics, and thus the values of density and power at which the transition from low to high mode occurs.

## II. EXPERIMENT

A schematic of the source chamber (7.9 cm D x 24 cm long) ECR apparatus is shown in Figure 1 and has been described elsewhere.[7] This system used a continuous-wave magnetron microwave generator (2.45 GHz) capable of operating from $P_{forward}$ = 0 to 800 W. The power was transmitted from a rectangular guide through a quartz window to the source chamber with an abrupt transition from the rectangular $TE_{10}$ to the circular $TE_{11}$ mode. For the purpose of these measurements, the tuning stub section of waveguide was effectively eliminated by positioning the stubs flush with the waveguide. We estimate from microwave theory

that $|r|^2$, the ratio of reflected to incident power contributed by the rectangular to circular waveguide transition without plasma, is approximately 0.15, which is relatively small. Forward power was measured using a 54 dB directional coupler with an HP 430C bolometer. Reflected power was measured at the dummy load with a Gerling calibrated crystal monitor. This measurement could only yield relative reflected power for low values ( <30 W) of reflected power. The current supplied to the magnets was variable and thus the magnitude of the dc B field was variable. Three magnetic field configurations were investigated in this study to examine the effects of the B field gradient at the resonance position, size of the resonance zone and number of resonance zones, on the low to high mode transition. The three on-axis B field magnitudes used are shown in Figure 2 along with a two dimensional representation of the ECR surfaces. The 150 A case had one broad resonance zone located at the mirror midplane in the center of the source chamber and the smallest normalized B field gradient at resonance, (1/B)(dB/dz), of the three cases. This magnetic field configuration was found to be the most stable with respect to ease of tuning and maintaining high mode under various plasma conditions and with gases other than argon. The 125 A case had two distinct resonance zones that were slightly sharper than the 150 A case. The 110 A case had one small volume resonance zone and the largest (1/B)(dB/dz) of the three cases investigated.

Experiments were performed using a moveable sliding short (ss) and axial E field and density probing. The ss was constructed from aluminum and solder-coated finger stock. The ss had 46 6.35 mm holes (to allow for vacuum pumping) and two larger slots for probe feedthroughs. Cylindrical Langmuir probe tips (7 mm long) were constructed from 0.076 mm D tungsten wire, and the probe body was fabricated with a right angle bend in order to have the wire perpendicular to the dc B field and parallel to the microwave E field. The ion density was estimated by applying a potential of approximately -60 V to the Langmuir probe and measuring the current drawn from the plasma. Under such probe bias conditions it was assumed that only ion current was being drawn.[8] The probe was kept at a constant position (6.3 cm from the window in the 150 A case, 10.2 cm in the 125A and 110 A cases) throughout each experiment at a fixed ss position in which the power was varied. Ion currents were measured for each ss position as a function of forward power ($P_{forward}$). The ion current was measured both as a function of increasing $P_{forward}$ and decreasing $P_{forward}$ to observe if the

ion density exhibited hysteresis.

The magnitude of the E field was measured by connecting the output of a probe to a crystal detector via a 20 dB microwave attenuator in a manner similar to Ref. 9. The subsequent crystal output dc signal was monitored with a voltmeter. The probe tip was rotated over an arc of 130° at each axial position to find the maximum signal. Probe measurements were taken at 6.35 mm increments along the axis of the chamber for each ss position.

## III. RESULTS

### A. Ion density measurements

From Laframboise's analysis[8], if the ion current to the probe is orbital motion limited and the probe radius over the Debye length is small, the current to a cylindrical probe follows the relation:

$$I_p = e n_i r_p l_p \left[\frac{-8eV_p}{M_i}\right]^{\frac{1}{2}} \qquad (1)$$

where $I_p$ is the measured ion current, $n_i$ is the ion density at the probe sheath edge, $r_p$ is the probe radius, $l_p$ is the probe length, $V_p$ is the probe bias, and $M_i$ is the ion mass. For our analysis, it was assumed that the primary ion was $Ar^+$. Figure 3 shows the ion density calculated from Eq. (1) vs. $P_{forward}$ and ss position for the three magnetic field configurations shown in Figure 2. For the 150 A magnet current (broad resonance zone case), two regions can be observed: a region below $P_{forward} \approx 40$ W (and below $n_{i,resonance} \approx 1 \times 10^{11}$ $cm^{-3}$) corresponding to low mode operation, and a region above $P_{forward} \approx 40$ W corresponding to high mode operation. The results for this case are repeated in Figure 4 on a linear scale showing an essentially linear increase in density with power at high input power. Calculations presented in Section IV indicate that nearly all of the incident power is absorbed by the plasma electrons under high mode conditions. Figure 4 also shows the much lower slope in the low power regime, with a transition to the higher slope occurring between $P_{forward} = 30$ to $P_{forward} = 40$ W. Linear regression of these data yields slopes of $1.2 \times 10^9$ $cm^{-3}$ $W^{-1}$ ($r^2 = 0.56$) for the low mode portion of the curve and $3.2 \times 10^{10}$ $cm^{-3}$ $W^{-1}$ ($r^2 = 0.95$) for the high mode portion, an increase

in slope of more than an order of magnitude. This indicates that in low mode only a small fraction of the incident power is absorbed in the plasma. As previously mentioned, quantitative reflected power values were not obtained at these low powers. Qualitatively, the reflected power for this case was found to decrease with increasing forward power in the transition region, dropping to near zero as high mode was achieved. The ion density was found to be independent of how the power was cycled and essentially independent of ss position. When the ss was within 1 cm of the resonance zone surface for this case (ss = 10.6 cm from the vacuum window) an ion density hysteresis with power was observed. When increasing the power from $P_{forward} = 0$, the plasma would not ignite until $P_{forward} = 120$ W. At this power level, the plasma appeared to jump directly into high mode. Upon decreasing the power, the plasma remained on and followed the same $n_i$ vs. $P_{forward}$ relation as seen at other sliding short positions. This may be due to the fact that a threshold breakdown field strength is required at the resonance zone to ignite the plasma, and when the ss is close to forcing a null at the resonance zone, it takes more input power to achieve this breakdown field. Once the plasma is ignited, the propagation characteristics of the chamber change enough that the plasma is able to be sustained below the ignition value.

The 125 A magnet current case yielded a different ion density vs. power curve, as is shown in Figure 3. The overall magnitude of the high mode plasma density was generally lower than the 150 A high mode case and a region of bi-stability was observed. The lower density can be attributed to several effects, one being the difference in position of the Langmuir probes with respect to the resonance zones in the two cases, and another due to the difference in sizes of the resonance zones. The overall decrease in ion density at constant pressure with decreasing resonance zone size has been previously observed in an oxygen plasma.[7] The ion density for the 125 A case was found to be bi-stable , i.e. rapidly jump between modes, in the power range of $65 \text{ W} < P_{forward} < 75 \text{ W}$. The ion density changed nearly an order of magnitude during these jumps, from $n_i \approx 5 \times 10^{10} \text{ cm}^{-3}$ to $n_i \approx 5 \times 10^{11} \text{ cm}^{-3}$. This case exhibited the same ion density vs. power hysteresis observed in the 150 A case when the sliding short was within 1 cm of the first resonance zone (i.e. the one closest to the vacuum window).

The 110 A magnet current case was similar to the 125 A case indicating a low to high mode jump

from $n_i \approx 5 \times 10^{10}$ cm$^{-3}$ to $n_i \approx 5 \times 10^{11}$ cm$^{-3}$, although the region of bi-stability was a function of the sliding short position. This magnetic field configuration also exhibited the ion density vs. power cycling hysteresis observed in both the 125 A and 150 A cases when the ss was close to forcing a null at the sharp resonance zone. However, unlike the other two magnetic configurations, the plasma became extinguished at relatively large power levels (i.e at $P_{forward}$ = 20 to 50 W, depending upon ss position) as the power was decreased below the ignition power value. Unlike the 150 A case, both the 125 A case and 110 A case showed increasing reflected power with increasing $P_{forward}$ in low mode, followed by a rapid drop to near zero once high mode was achieved. This result, which has been observed in other systems[6], is not understood.

Figure 5 shows the axial ion density profile for the 110 A magnet current case in low mode. The density sweep was taken at $P_{forward}$ = 25 W when possible. At some ss positions, the plasma could not be sustained at this low power; thus a slightly higher power was used. The ion density peaks at or very near the resonance zone for all ss positions. The density at the vacuum window and near the ss was significantly lower than that observed in the ECR zone, indicative of diffusive axial ion loss. Axial ion density scans for the other two magnetic field cases yielded similar ion density profiles, although the maximum ion density was more broadly distributed than observed in Figure 5, which correlates to the larger resonance volumes. The radial density was found to have a roughly parabolic shape over the diameter. As the ion Larmor radius, $a_i$, at the electron temperature is approximately 0.13 cm, which is approximately 20% or less of the ion mean free path along the field, and the radial and axial density gradients are similar, we expect that the radial diffusion plays little role in the dynamics.

**B. E probe results**

The axial E field intensity vs. sliding short position for the 150 A magnetic field configuration can be seen in Figure 6. All intensity measurements were taken in low mode and $P_{forward}$ = 25 W. The ion density measured at the fixed position shown in Figure 3 under these conditions was essentially constant throughout these measurements. It is clear from these data that there are two distinct regions in the source chamber; one pre-resonance zone (i.e. between the vacuum window and the resonance zone) and one post-resonance zone. The field structure in the post-resonance zone is dominated by the position of the sliding short. This can be

readily seen by tracking the position of the E field maxima labeled "A" and "B" in Figure 6. If a simple standing wave pattern exists in the source chamber and the sliding short is a forced E field null, then the "A" peak always should be 1/4 wavelength in front of the sliding short. The "A" peak was found in front of the sliding short, but the sliding short to "A" peak distance varied somewhat with ss position. This distance tended to be about 3.5 cm, but it appeared to be as close as 2 cm for some ss positions. The "B" peak is similarly moveable maintaining a roughly constant distance from the short. The portion of the pre-resonance zone E field maximum, "C," did not move significantly with the position of the sliding short at constant power, but the intensity of this peak did vary with sliding short position.

Figure 7 shows the 125 A magnetic field configuration E field intensity vs. position results. This case varies from the 150 A case in that instead of one broad resonance zone located at the mirror midplane of the source chamber, there were two sharper resonance zones. The second zone does not appear to effect the E field structure inside of the source chamber. As was the case for the 150 A configuration, there is always a pre-ss peak, "A," located in front of the sliding short as it moved towards the vacuum window. (The 18.1 cm ss position data do not show an "A" peak. A peak was observed but the proximity (within 2 cm) of the short prevented accurate intensity vs. position measurement.) Again, the sliding short to "A" peak distance and the "A" peak intensity varied with sliding short position, just as in the 150 A case. The pre-first resonance zone peak, "C," also acted very similar to the 150 A case. The middle peak, "B," was small or not observed in several of the sliding short positions, and was generally much further from the "A" peak than for the 150 A case.

The 110 A magnetic field case data is shown in Figure 8. As was mentioned in discussion of the ion density vs. power results, the ability to sustain the plasma was strongly influenced by the position of the sliding short. Consequently, a $P_{forward} = 25$ W plasma could not be sustained at all sliding short positions. Thus the power at which each of the E field sweeps were taken is shown in Figure 8. Unlike the previous two cases, a strong E field peak directly in front of the sliding short was not always observed. Also unlike the previous two cases, there was a sliding short position far removed (13 cm) from the resonance zone that prevented the plasma from being ignited, even at 800 W forward power. The vacuum field for this case is shown in Figure

8 for the 18.1 cm sliding short position. From this data it can be seen that a broad E field null is located around the sharp resonance zone and is apparently preventing plasma ignition. The intensity of the vacuum E field was also found to be nearly an order of magnitude greater than the magnitude measured with a plasma present for the same forward power. This may indicate that the measurement technique may be sensitive to large variations in plasma density.

Figure 9 shows the high mode E field intensity vs. position curves for the 125 A and 150 A magnetic field cases at 75 W and 21.9 cm sliding short position. All of the post resonance zone E field structure disappears at the onset of high mode (as determined from the ion density measurements). The disappearance of the E field is generally correlated with the resonance zone, indicative of strong power absorption in this zone. The extent of the field decay is probably due to both the nonlinear absorption effects and to the fact the resonance zones are really surfaces and extend on either side of the axial ECR resonance point. Measurements at other plasma conditions indicate that the general structure observed in Figure 9 is always observed in high mode.

## IV. DISCUSSION

The general results are consistent with the picture that above a critical density the power transmitted into the ECR zone is nearly totally absorbed in the zone. This power must then be lost through various channels. These loss channels include electron and ion loss to the walls, excitation energy, elastic scattering collisional losses inside the plasma and losses due to ionization.[10] These losses must balance the input power at the equilibrium ion density. Assuming that the majority of power is absorbed by electrons in the resonance zone, and given that the ion density was maximum at or near the resonance zones in all of the cases examined, the majority of the input power is absorbed and redistributed into ionization energy, collisional losses and energy of the electrons and ions in a small volume enclosing the resonance zone (3-5 cm wide). Thus, a power balance can be made about this arbitrary control volume enclosing the resonance zone. A simple formulation of this power balance gives the following relation:

$$P_{abs} = n_i u_i A_{CV}(e\,\varepsilon_L) \tag{2}$$

where $n_i$ is the density at the control volume edge, $u_i$ is the ion velocity at the control volume edge, $A_{CV}$ is the surface area of the control volume and $(e\varepsilon_L)$ is the effective energy lost per electron-ion pair created in the control volume. This loss term combines the electron energy lost through the channels listed above with the energy of each particle leaving the control volume per unit time. This loss term is primarily a function of the electron temperature of a gas through the cross sections for collisional, excitation and ionization processes. For argon with electron temperatures near 4 eV, the loss term should be 40-60 eV.[10] Assuming that the magnetic field is sufficiently strong and the pressure is sufficiently low in the control volume to minimize significant radial ion loss to the walls, then twice the cross--sectional area of the source chamber can be used as $A_{CV}$. An estimate of the ion velocity across the control volume edge can be made by calculating the energy gained by the ion as it falls through the distributed sheath (the potential drop due to the density difference between the resonance zone and the control volume edge) and solving for the velocity.[11] Thus, the ion velocity can be expressed as:

$$u_i = \left[\left(\frac{2kT_e}{eM_i}\right)\ln\frac{n_{i,res}}{n_{i,CVedge}}\right]^{\frac{1}{2}} \tag{3}$$

Substituting the average ion density at the control volume edge for a given forward power (thus assuming full power absorption) for any of the high mode cases and using Eq. (3) to calculate the ion velocity, one obtains between 35 and 60 V for the energy loss factor in Eq. (2). This is in good agreement with the expected value.

Below the critical density there is a transition to a lower density state at which the plasma is nearly transparent to the standing waves that penetrate into the chamber resulting from reflections within the ECR source chamber. A qualitative understanding of this phenomenon comes from the theory of absorption in a resonance layer of the right hand circularly polarized (RHP) plane wave, when propagating from the region where $\omega_c > \omega$ to $\omega_c < \omega$. Here $\omega$ is the applied frequency and $\omega_c = eB/m$ is the electron cyclotron frequency. In the simple configuration of a uniform density plasma and a linearly decreasing B field near resonance, Budden[12] has calculated that the fraction of the input power absorbed when passing through resonance is

given by:

$$P_{abs} = P_{input}(1-e^{-\pi\eta}) \tag{4}$$

where

$$\eta = \frac{\omega_p^2}{\omega c \alpha} \tag{5}$$

In Eq. (5) $\omega_p^2 = e^2n/m\epsilon$ is the square of the radian plasma frequency, $\alpha$ = (1/B)(dB/dz) is the normalized magnetic field gradient at the resonance position, and c is the velocity of light. In the experiment, $\alpha$ varied from nearly 0 at the 150 A magnetic field case (where Budden's theory does not apply) to 0.1 $cm^{-1}$ for the 110 A case. Using the value of 0.1 $cm^{-1}$ for $\alpha$ and setting $\pi\eta = 1$ (i.e. $(1-e^{-1})$ of the RHP power absorbed) one finds that the plasma density at the resonance zone for a transition from low to high mode should be approximately $5 \times 10^9$ $cm^{-3}$ - a value more than an order of magnitude below the lower value of density observed in our system at the transition. Indeed, for a value of $n_i = 1 \times 10^{10}$, $\eta = .69$ and $P_{abs} = 0.89\ P_{input}$.

Clearly, the Budden theory is too idealized for application to our system in a number of respects. The reflections in the chamber generate interference of waves at field nulls that can significantly affect the absorption. The variation of axial plasma density noted in Figure 5 causes initial upstream power reflection not included in the Budden theory. In addition, the waves are not propagating parallel to the magnetic field due to the transverse separation constant in the cylindrical ECR chamber. These and other factors can be taken into account by numerically integrating the wave equation in the varying magnetic fields and densities characteristic of the experiment. Preliminary calculations of this type have been carried out, qualitatively indicating that many of the features that are observed experimentally.[13] However, the transitions from high absorption to low absorption still occur at densities in the range of those calculated by the Budden theory, rather than the higher densities measured experimentally. This discrepancy has not been resolved.

The pattern of the electric field in front of the moveable short is generally consistent with the Budden theory but also has some unexplained features. In the vacuum guide, the axial propagation constant is given

by:

$$k_g^2 - k_o^2 - k_c^2 \tag{6}$$

where $k_o$ is the free space propagation constant at f=2.45 GHz and $k_c$ is the transverse separation constant of the $TE_{11}$ mode in the 7.9 cm D circular guide. This gives a free space guide wavelength, $\lambda_g$, of 26.6 cm. With the plasma filled waveguide, in a simple approximation, we replace $k_o^2$ in Eq. (6) with $k^2$ given by:

$$k^2 - k_o^2\left[1 - \frac{\omega_{pe}^2}{\omega\,(\omega - \omega_c(z))}\right] \tag{7}$$

For the RHP wave, $\omega_c > \omega$, giving a larger $k^2$ and therefore a smaller guide wavelength in the absence of the plasma. The exact values depend on the detailed density and magnetic field profiles. In the 150 A magnet current case, $\omega_c > \omega$ and the value of $\lambda_g/4 \approx 4$ cm is not unreasonable far from the resonance. Nearer the resonance, e.g. with the ss at 14.3 cm, the resonant denominator in Eq. (7) increases k, therefore shortening $\lambda_g/4$, as observed. In the 125 A and 110 A cases, $\omega_c < \omega$ beyond the resonance, so that the wave is non-propagating over much of the distance between the resonance and the short. The complicated field patterns would not be easy to interpret for these cases. However, the hysteresis generated by the sliding short field nulls can be qualitatively understood in terms of the change in guide wavelength with plasma density.

The fixed positions for peaks in the field upstream of the resonance indicate the importance of reflections in this region from both the rapidly changing plasma density (as is seen in Figure 5) and possibly the impedance mismatch at the transition from rectangular to circular guide. These effects are not included in the uniform density Budden model, but would clearly be expected to play a role in determining the fraction of the power absorbed. In numerical integration of the wave equation, reflections due to plasma density variations are quite evident. An effect of plasma loading of the source chamber is to lower the wave impedance via the shortening of the plasma guide wavelength as described by Eqs. (6) and (7). Since the impedance of the circular guide is higher than the rectangular guide under vacuum conditions, plasma loading initially improves the match until approximately $\omega_p \approx 0.5\ \omega$, $n_i \approx 2 \times 10^{10}$ cm$^{-3}$, after which the discontinuity

again increases. Transitions from low to high mode were also observed in a 2.45 GHz ECR source in a 14.6 cm D chamber propagating a $TM_{01}$ mode with a low reflection matching section from the waveguide and have been observed elsewhere.[4] The difference in mode structure and lack of reflections at the waveguide--to--source chamber transitions indicated that these factors do not play an essential role in the process.

## V. CONCLUSIONS

The low-to-high mode plasma transition in an argon ECR plasma has been characterized by electrostatic Langmuir probing and axial E field intensity mapping as functions of the position of a sliding short and magnetic field configuration. The power and ion density for the mode transition were found to be nearly independent of ss position in the source chamber, except when the ss forced a null in the neighborhood of the resonance zone. The ion density vs. forward power cycling curves exhibited two distinct slopes for the high and low mode regions for the 150 A magnetic field case, which had the largest resonance zone. The high mode ion density vs. $P_{forward}$ slope was consistent with absorption of nearly all of the incident power in the plasma and was more than an order of magnitude greater than the low mode slope. The transition between these two modes occurred at approximately 40 W, which agreed with the E probe transition, indicating that little power was transmitted through the resonance zone. The other two magnetic field configurations yielded ion density vs. power curves which exhibited a bi-stability in the low to high mode transition. The magnitude of the on-axis ion density near the resonance zone during this transition was for all cases approximately 5 x $10^{10}$ $cm^{-3}$ in low mode jumping to approximately 5 x $10^{11}$ $cm^{-3}$ in high mode. This transition was more gradual, however, in the 150 A case. All three magnetic field configurations exhibited ion density hysteresis on power cycling when the ss forces an E field null near the resonance zone. The low mode E field structure inside the source chamber was found to have two distinct regions, one pre- and one post-resonance zone for all magnetic field configurations. The position of the E field maxima varied with ss position in the post-resonance zone as would be expected from a forced null at the ss position. The field intensity pre-resonance zone did not vary in position as a function of ss position, but did vary in intensity. The post resonance E field structure at constant ss position decreased abruptly with increasing power as the ion density jumped into the

high mode. This transition occurred when $P_{forward}$ was increased past 40 W for the 150 A magnetic field case, essentially independent of the ss position, while for the 125 A and 110 A cases it occurred at somewhat higher power and varied with ss position. These results indicate that the magnetic field design for the largest range at which high densities can be achieved and one that is least sensitive to internal reflections should have a large volume ECR resonance zone.

ACKNOWLEDGEMENTS

This work was supported by National Science Foundation Grant Nos. ECS-8517363 and ENG-8710988, Department of Energy Grant NO. DE-FG03-87ER13727, and contracts from IBM General Technology Div., Burlington, VT and Applied Materials Corp., Santa Clara, CA. The authors would like to thank J. Steinhauer for probe fabrication and assistance in initial low/high mode measurements, R. J. Lynch for his help with the data acquisition, and R. A. Stewart for helpful discussions on low/high mode behavior in large diameter ECR systems with $TM_{01}$ launched input power.

REFERENCES


1. J. Asmussen, *J. Vac. Sci. Tech.* A 7, 883 (1989) and references within.

2. O. A. Popov, *J. Vac. Sci. Tech.* A 7, 894 (1989).

3. E. Ghanbari, I. Trigor and T. Nguyen, *J. Vac. Sci. Tech.* A 7, 918 (1989).

4. S. M. Gorbatkin, L. A. Berry and J. B. Roberto, *J. Vac. Sci. Tech.* A 8, 2893 (1990).

5. C. C. Tsai, L. A. Berry, S. M. Gorbatkin, H. H. Haselton and W. L. Stirling, *J. Vac. Sci. Tech.* A 8, 2900 (1990).

6. O. A. Popov, *J. Vac. Sci. Tech.* A 8, 2909 (1990).

7. D. A. Carl, D. W. Hess and M. A. Lieberman, *J. Vac. Sci. Tech.* A 8, 2924 (1990).

8. J. G. Laframboise, *Inst. for Aeronautics Report #100*, Section 14 (1966).

9. J. Hopwood, R. Wagner, D. K. Reinhard and J. Asmussen, *J. Vac. Sci. Tech.* A 8, 2904 (1990).

10. G. R. Misium, A. J. Lichtenberg, and M. A. Lieberman, *J. Vac. Sci. Tech.* A 7, 1007 (1989).

11. D. A. Carl, D. W. Hess and M. A. Lieberman, *J. Appl. Phys.* **68** 4, 1863 (1990).

12. K. G. Budden, **Radio Waves in the Ionosphere**, Cambridge (England) University Press, 474-479 (1966).

13. D. A. Carl, A. J. Lichtenberg, M. A. Lieberman, J. Steinhauer and M. C. Williamson, "Power Absorption by Electron Cyclotron Resonance," Abstract NA-5, *42nd Annual Gaseous Electronics Conference*, 17-20 October 1989, Palo Alto, CA, p. 163.

## FIGURE CAPTIONS

Fig. 1: Schematic of the ECR system

Fig. 2: Magnetic field magnitude as a function of position and magnetic current for the three field geometries and currents investigated, along with a two dimensional representation of the resulting ECR surfaces.

Fig. 3: Ion density (logarithmic scale) vs. $P_{forward}$ for both increasing and decreasing power sweeps as a function of ss position for all three magnetic field configurations.

Fig. 4: Detail of 150 A ion density (linear scale) vs. $P_{forward}$ during low to high mode transition.

Fig. 5: Ion density vs. axial position in the ECR source chamber as a function of ss position in low mode for the 110 A case.

Fig. 6: Axial E field intensity versus position for various ss positions for low mode, $P_{forward}$ =25 W, 150 A magnetic current case. The ss position was varied from 21.9 cm to 10.6 cm.

Fig. 7: Axial E field intensity versus position for various ss positions for low mode, $P_{forward}$ =25 W, 125 A magnet current case.

Fig. 8: Axial E field intensity versus position for various ss positions for the low mode 110 A magnet current case.

Fig. 9: Axial E field intensity vs. position in high mode for two magnetic field configuration and one ss position.

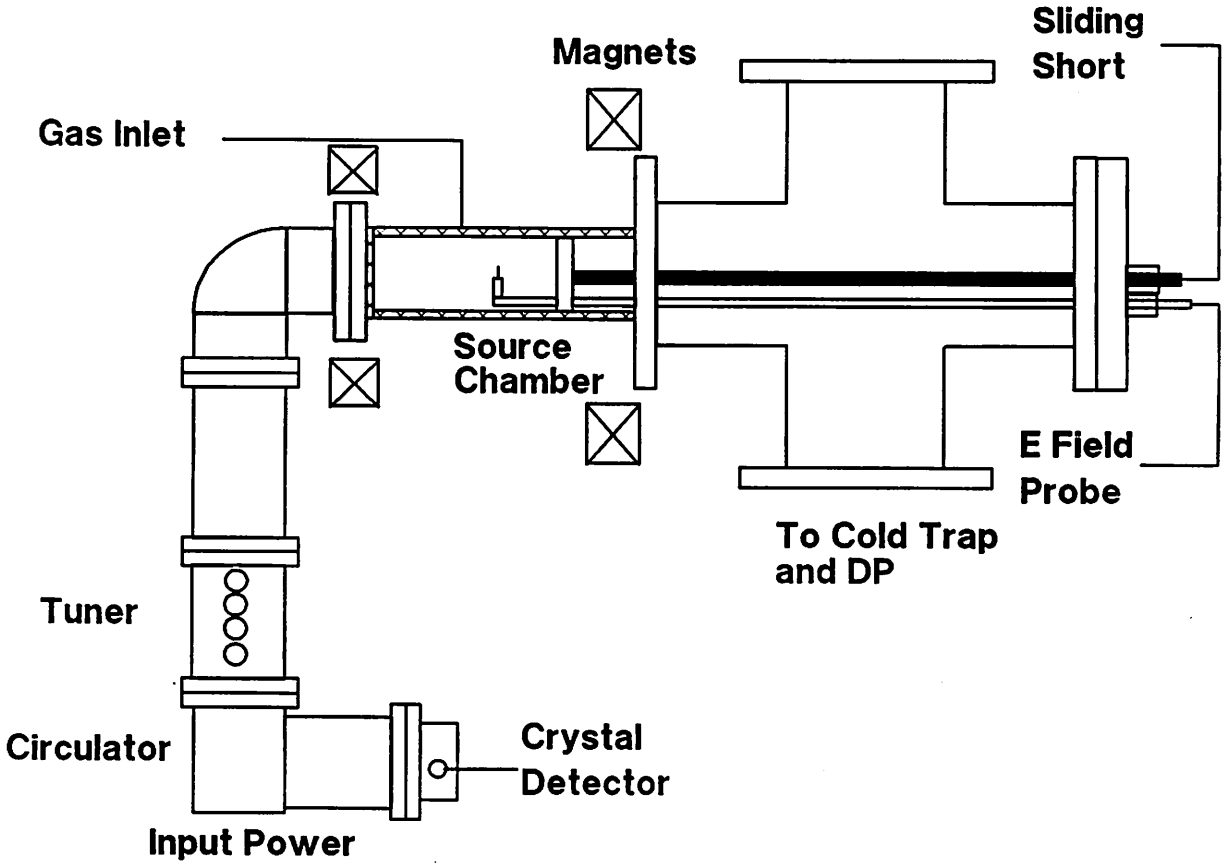
Sliding
Short
Magnets
Gas Inlet
Source
Chamber
E Field
Probe
To Cold Trap
and DP
Tuner
Circulator
Crystal
Detector
Input Power

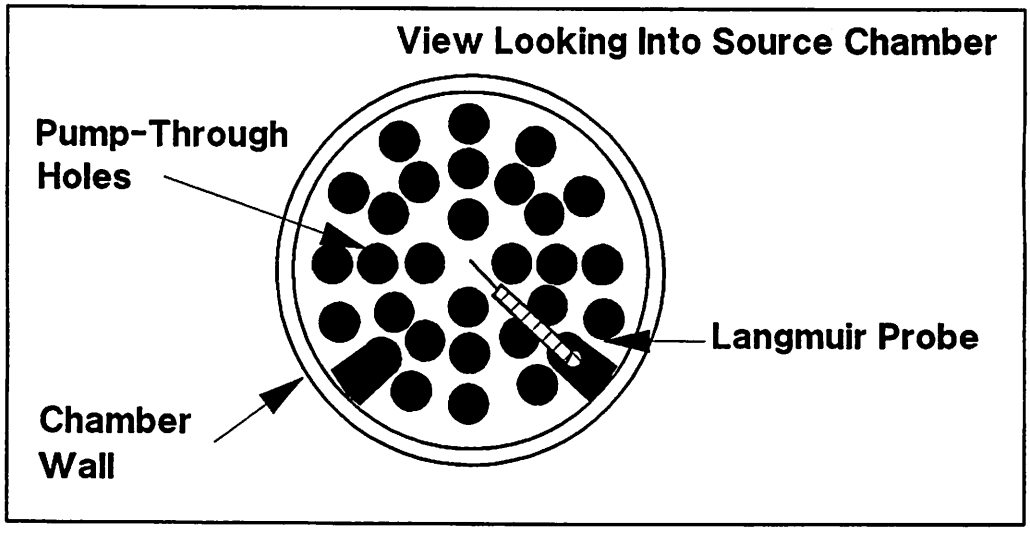
View Looking Into Source Chamber
Pump-Through
Holes
Langmuir Probe
Chamber
Wall

Figure 1

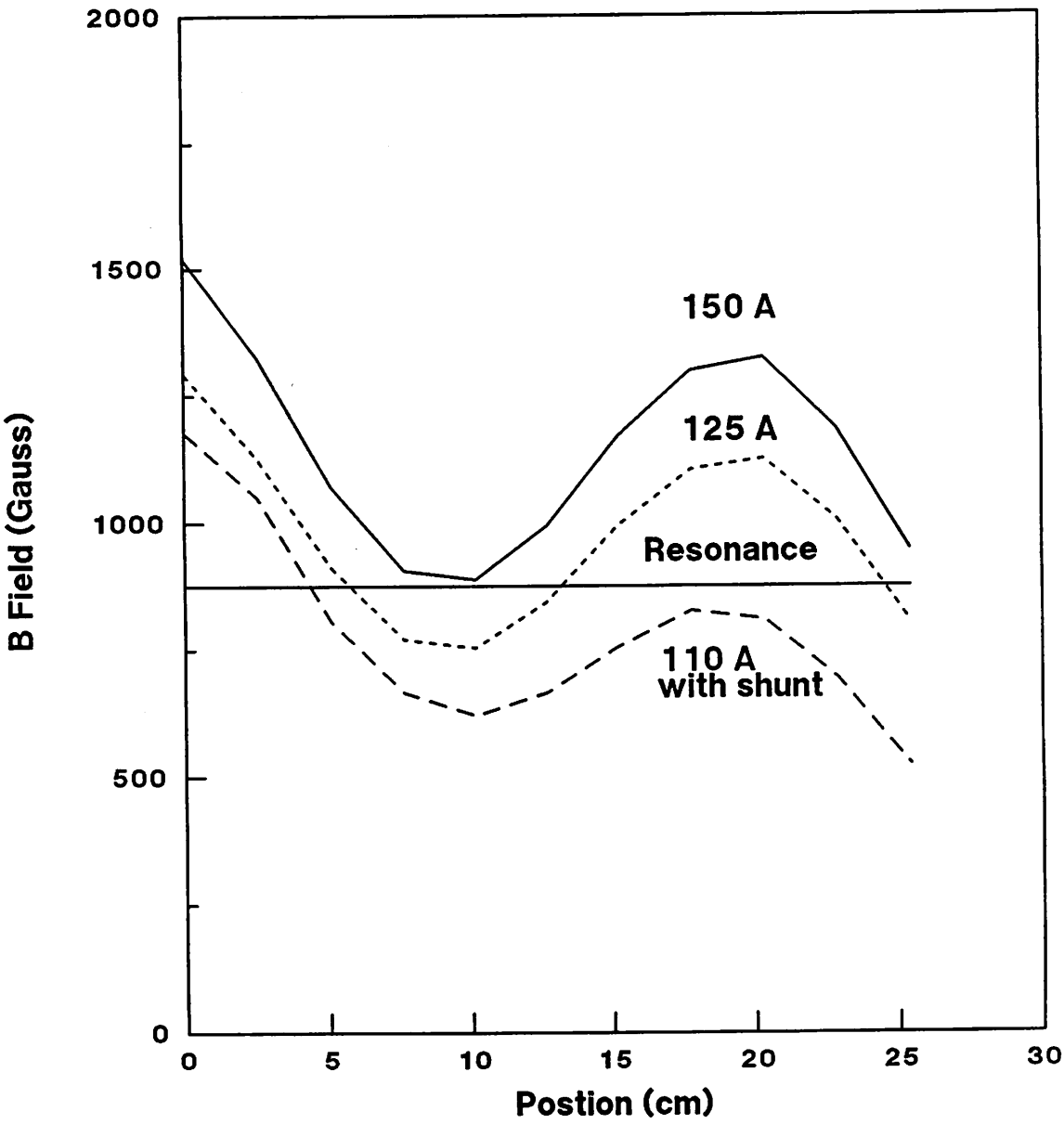


Figure 2
(Part I)

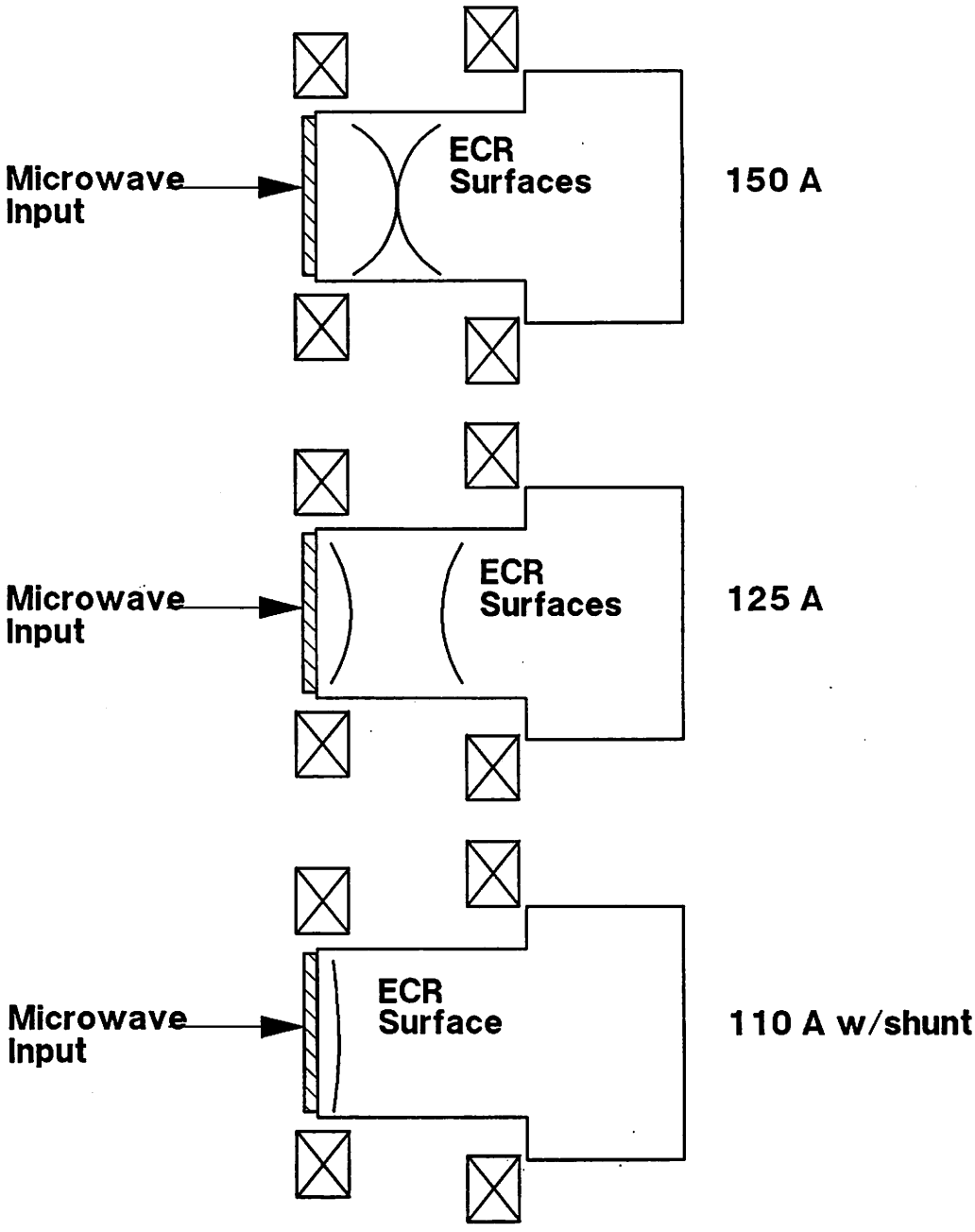


Figure 2
(Part II)

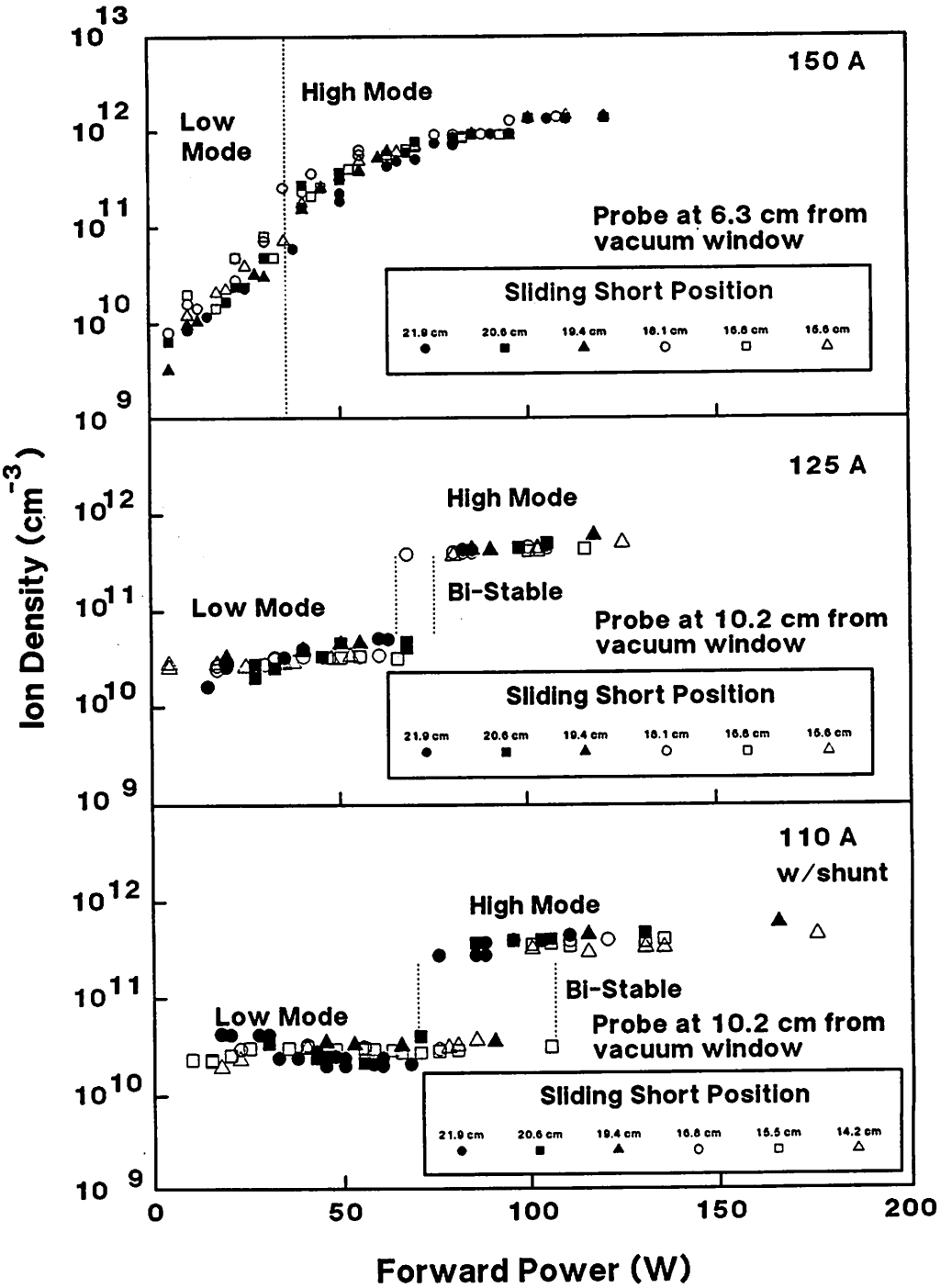
150 A
High Mode
Low Mode
Probe at 6.3 cm from vacuum window
Sliding Short Position
21.9 cm
20.6 cm
19.4 cm
18.1 cm
16.8 cm
15.6 cm
125 A
High Mode
Bi-Stable
Low Mode
Probe at 10.2 cm from vacuum window
Sliding Short Position
21.9 cm
20.6 cm
19.4 cm
18.1 cm
16.8 cm
15.6 cm
110 A
w/shunt
High Mode
Bi-Stable
Low Mode
Probe at 10.2 cm from vacuum window
Sliding Short Position
21.9 cm
20.6 cm
19.4 cm
16.8 cm
15.5 cm
14.2 cm
Ion Density (cm-3)
Forward Power (W)
0
50
100
150
200

Figure 3

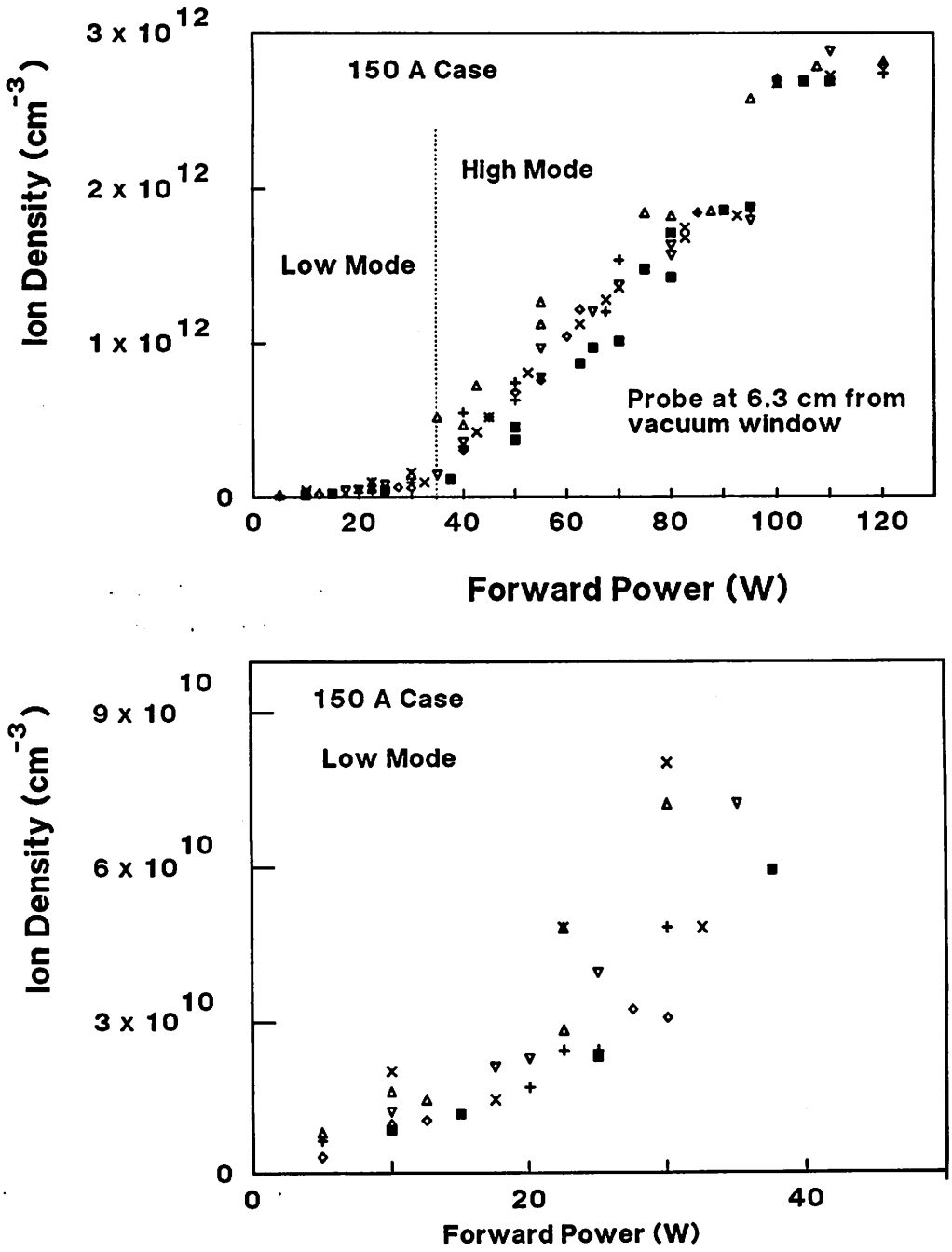
150 A Case
High Mode
Low Mode
Probe at 6.3 cm from vacuum window
Ion Density (cm-3)
3 x 10 12
2 x 10 12
1 x 10 12
0
0
20
40
60
80
100
120
Forward Power (W)
150 A Case
Low Mode
Ion Density (cm-3)
9 x 10 10
6 x 10 10
3 x 10 10
0
0
20
40
Forward Power (W)

Figure 4

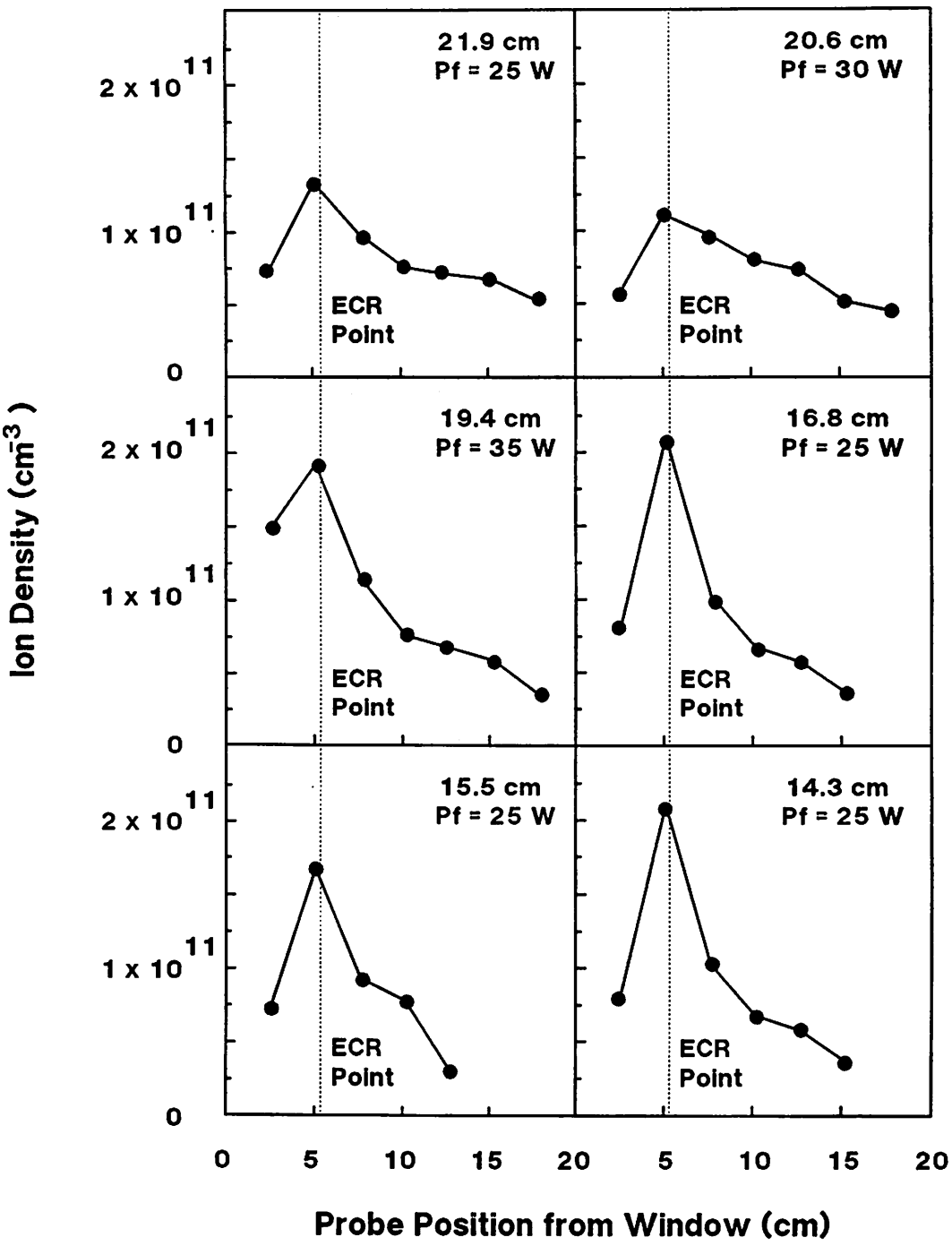


Figure 5
(Part I)

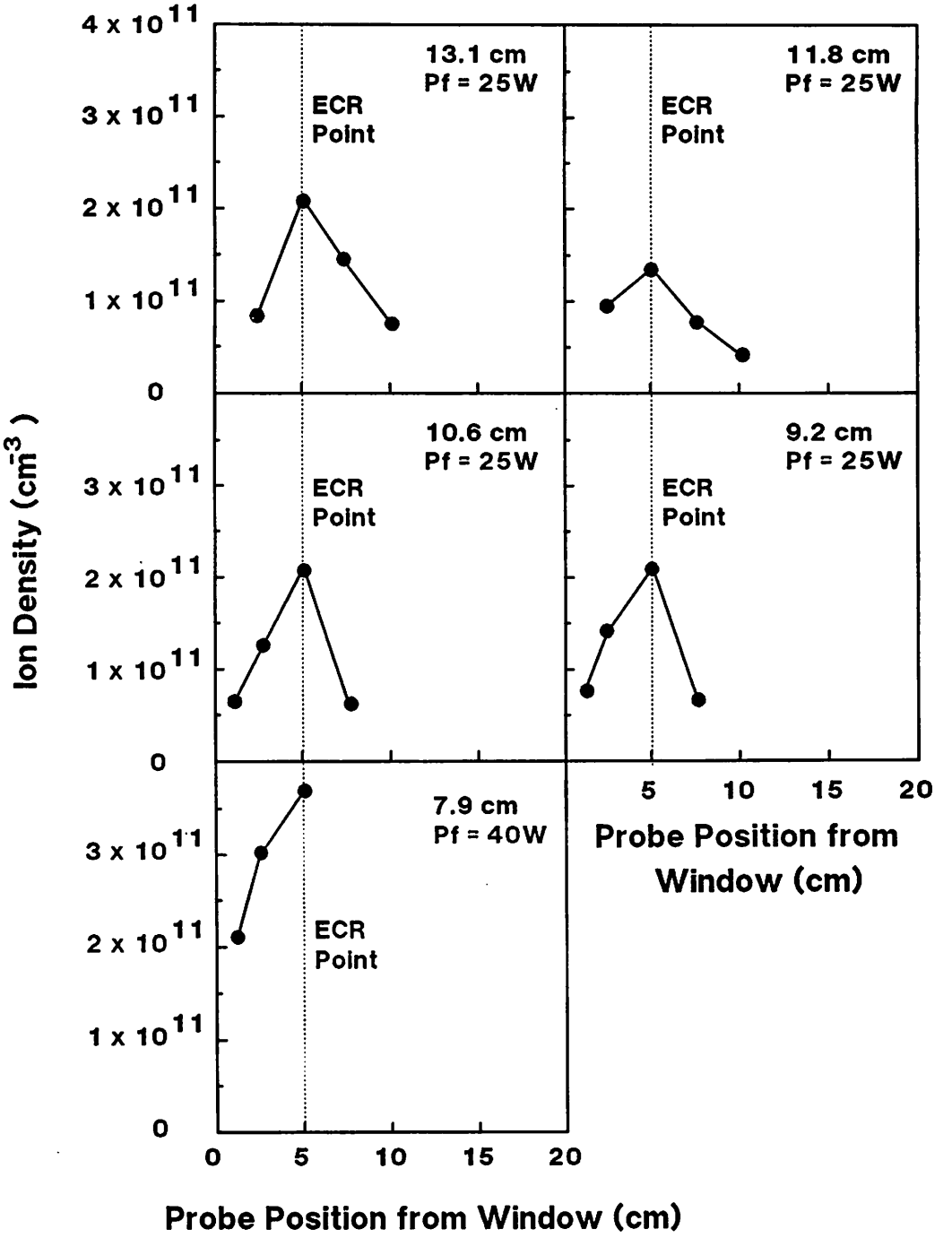


**Figure 5**
**(Part II)**

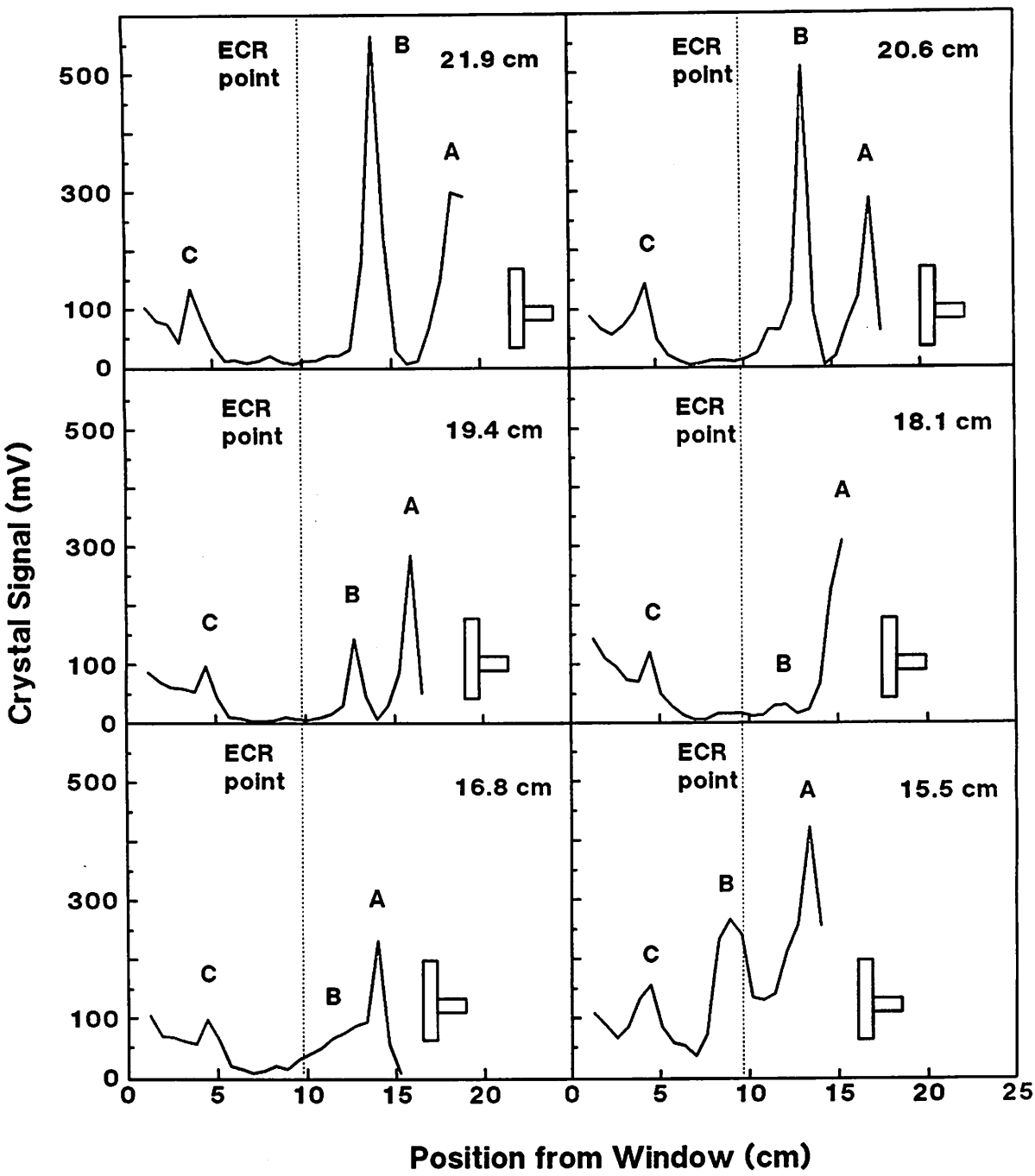


Figure 6
(Part I)

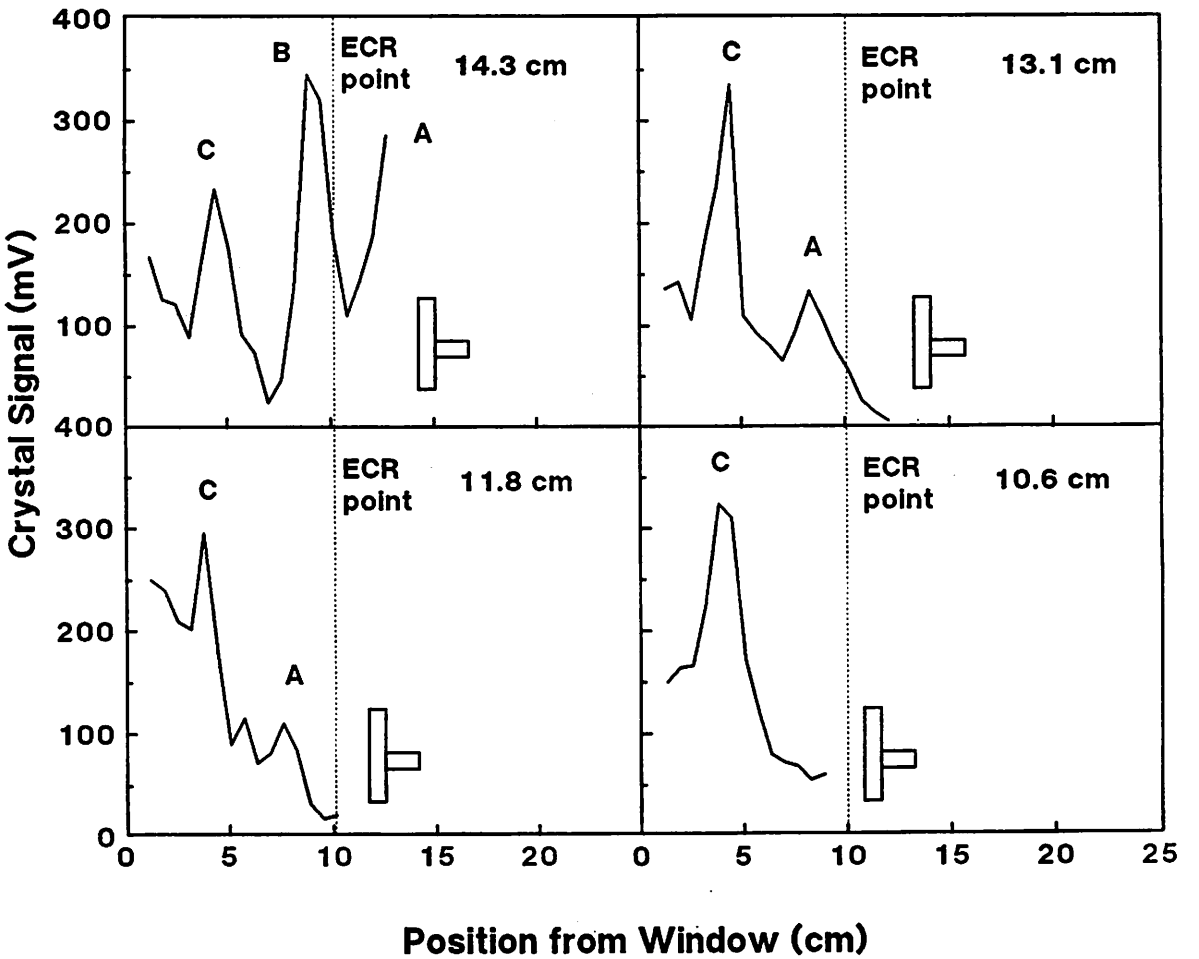


**Figure 6**
**(Part II)**

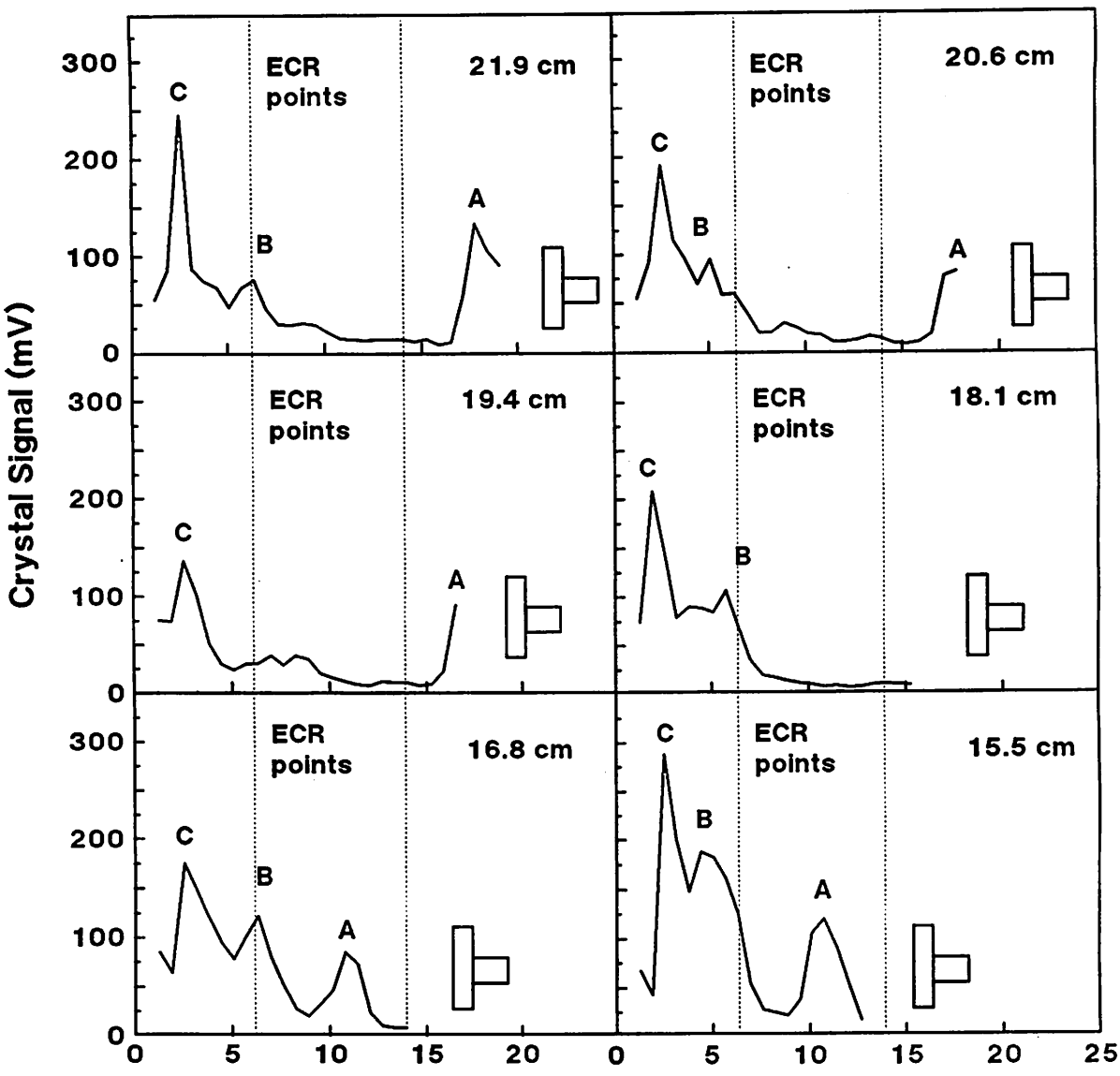


**Figure 7**
**(Part I)**

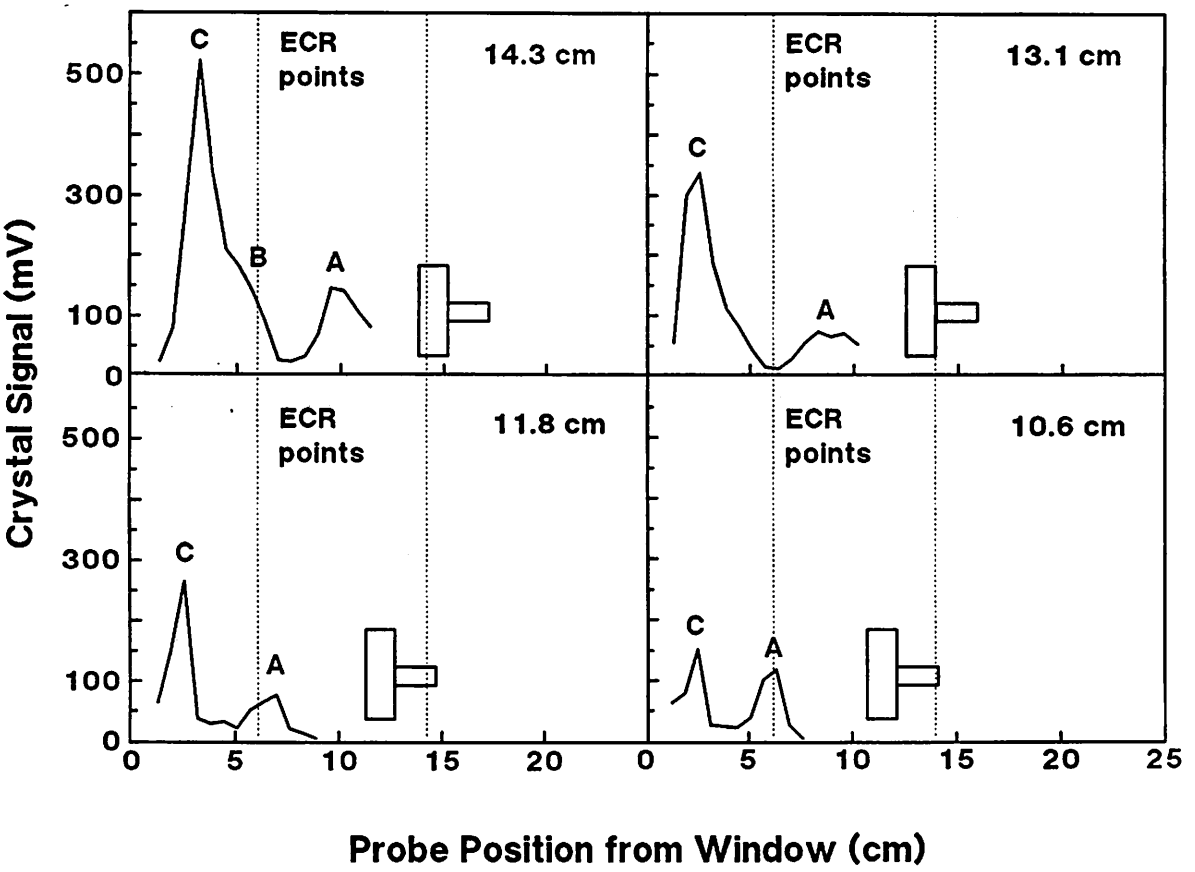


Figure 7
(Part II)

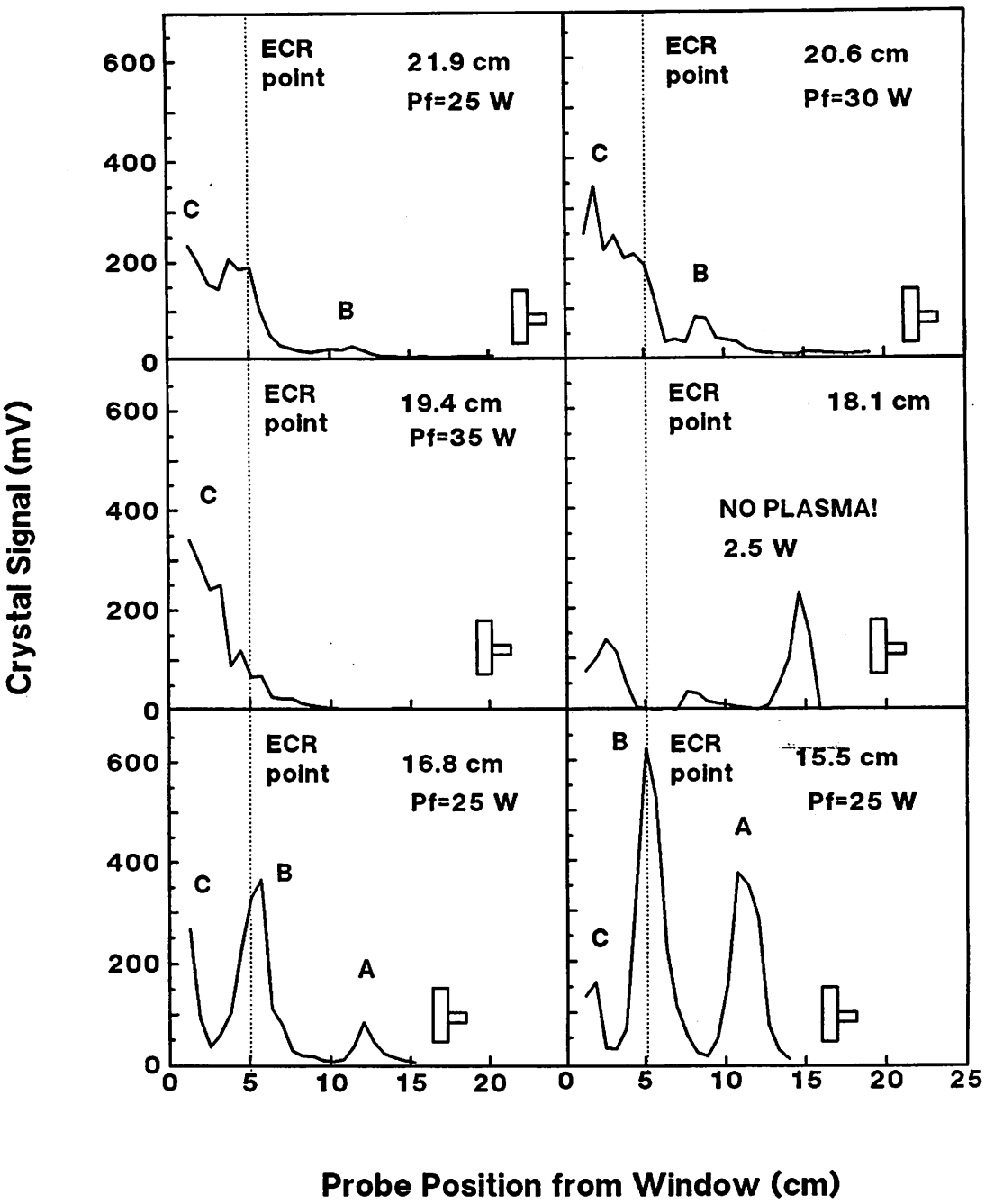


Figure 8
(Part I)

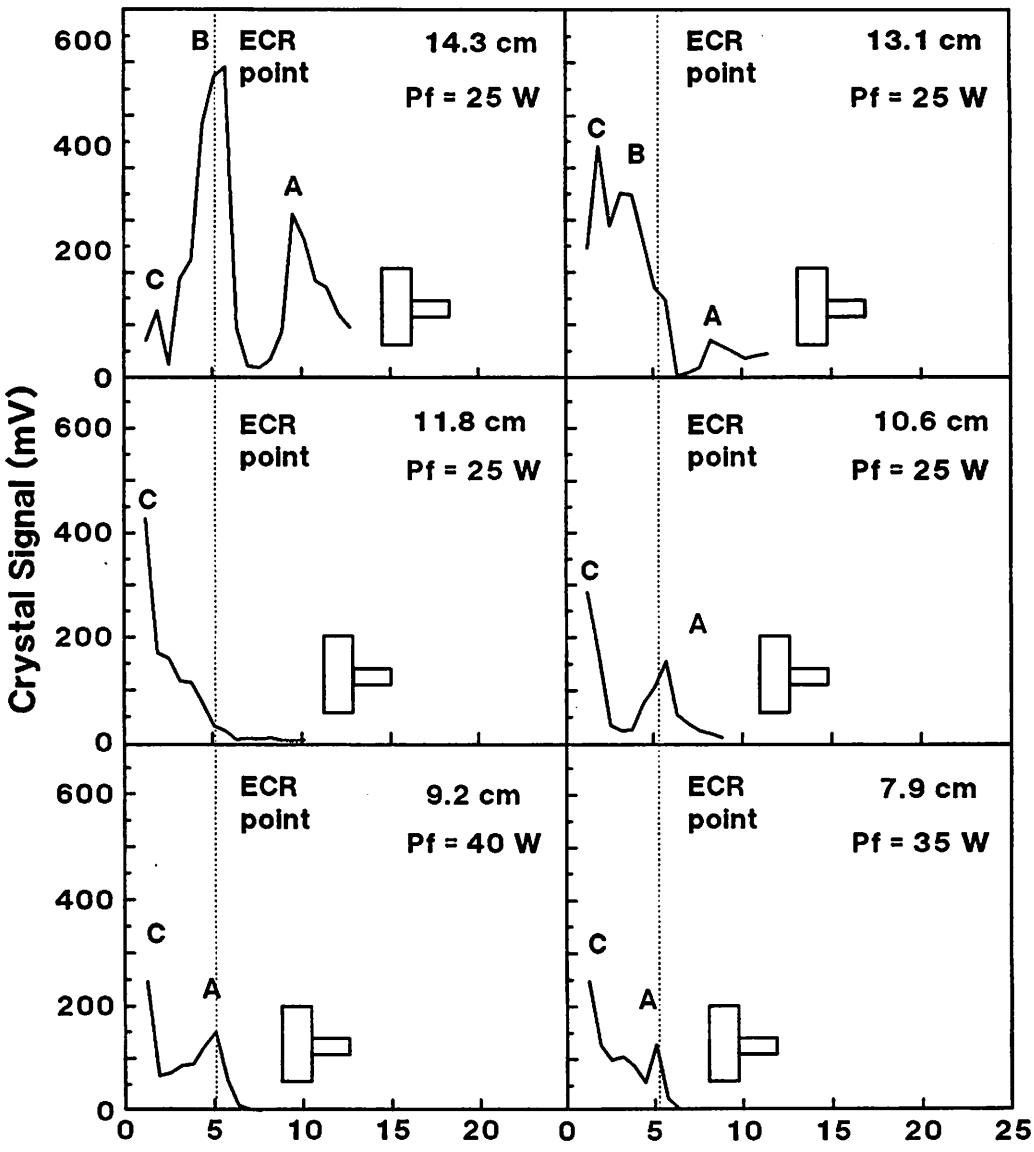


**Figure 8**
**(Part II)**

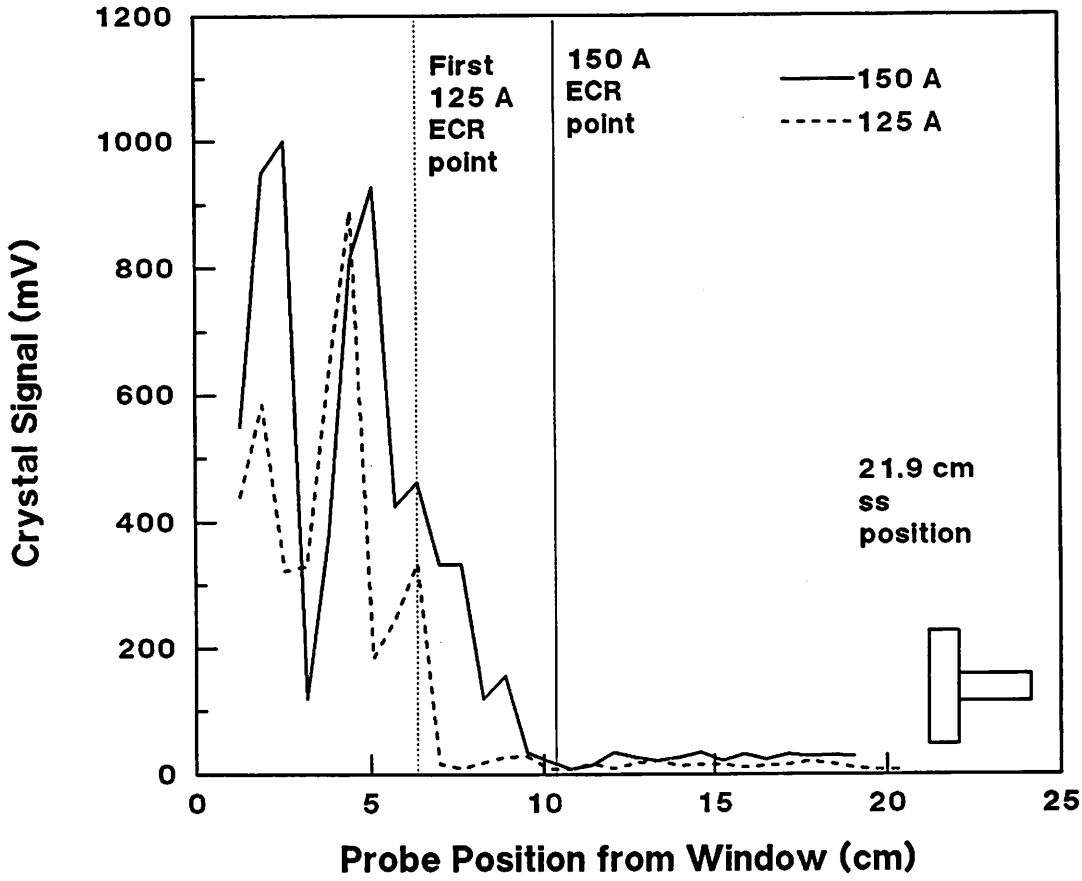
1200
1000
800
600
400
200
0
Crystal Signal (mV)
0
5
10
15
20
25
Probe Position from Window (cm)
First
125 A
ECR
point
150 A
ECR
point
150 A
125 A
21.9 cm
ss
position

Figure 9